Journal of Structural Geology, Vol. 15, No. 9/10, pp. 1249 to 1256, 1993
Printed in Great Britain

0191-8141/93 $06.00+0.00
Pergamon Press Ltd

The rheology of faults triggered by the olivine–spinel transformation in Mg_2GeO_4 and its implications for the mechanism of deep-focus earthquakes

TRACY N. TINGLE* and HARRY W. GREEN, II†

Department of Geology, University of California, Davis, CA 95616, U.S.A.

and

CHRISTOPHER H. SCHOLZ and T. A. KOCZYNSKI

Lamont-Doherty Earth Observatory of Columbia University, Palisades, NY 10964, U.S.A.

(*Received* 2 *July* 1992; *accepted in revised form* 4 *December* 1992)

Abstract—The relevance of the anticrack faulting mechanism to the origin of deep-focus earthquakes depends critically on the physical processes operating during fault generation and movement. We show here that the resistance to sliding on fault zones produced by this mechanism in Mg_2GeO_4 depends only weakly on confining pressure, but strongly on sliding rate. Both of these characteristics are inconsistent with friction. The microstructures of the fault zones and the crystal-plastic rheology of the constituent phases indicate that sliding must occur primarily by grain-boundary sliding. Previously, we reported that anticrack faulting is accompanied by elastic radiation of energy (acoustic emissions), and that it can operate during the $\alpha \rightarrow \beta$ transformation in $(Mg,Fe)_2SiO_4$ at the pressures and temperatures at which deep earthquakes occur. The present results and the recent demonstration that metastable olivine is present in the subducting slab beneath Japan provide additional support for the anticrack theory of deep-focus earthquakes.

INTRODUCTION

DEEP-FOCUS earthquakes have been a paradox since their discovery 70 years ago. Their seismic characteristics are virtually indistinguishable from those of shallow earthquakes, yet experimental evidence and theoretical considerations demonstrate that brittle shear fracture and stick–slip frictional sliding, the physical mechanisms responsible for shallow earthquakes, cannot operate at the high pressures at which deep earthquakes occur. Thus, it has been argued almost since their discovery that deep earthquakes must be the result of a different process. Kirby (1987) suggested that some peculiar aspects of faulting at high temperatures and high pressures in tremolite and at low temperatures and low pressures in H_2O ice may be relevant. He argued that incipient transformation to the more dense higher pressure assemblage may have triggered faulting, although the actual mechanism by which this process could occur remained unclear.

Observations of microstructures in Mg_2GeO_4 olivine polycrystals that exhibited anomalous faulting behavior at high pressure (0.8–2.2 GPa) led to the proposal that faulting occurs by incipient transformation of metastable olivine to very fine-grained spinel in lens-shaped Mode I microanticracks that organize themselves into throughgoing faults on which sliding occurs by superplastic deformation of the fine-grained spinel (anticrack theory of phase-transformation faulting; Green & Burnley 1989, Burnley *et al.* 1991). The same microstructures and anomalous faulting behavior also have been observed at 14 GPa in association with the $\alpha \rightarrow \beta$ phase transformation in $(Mg,Fe)_2SiO_4$ olivine in peridotite of appropriate composition for the Earth's mantle, supporting the hypothesis that this is the mechanism of deep-earthquake faulting (Green *et al.* 1990). Subsequent investigations of the faulting phenomenon in ice have revealed microstructures similar to those present in the germanate specimens (Kirby *et al.* 1991).

Despite its remarkable similarity to brittle shear fracture, several aspects of the anomalous faulting behavior in Mg_2GeO_4 indicate that it is not a brittle phenomenon. Principal among these are the following. (1) There are no detectable acoustic emissions prior to failure (Green *et al.* 1992). (2) The faulting stress is independent of confining pressure (Burnley *et al.* 1991). (3) Faulting occurs only in a narrow temperature window (Burnley *et al.* 1991). (4) Very fine-grained spinel is present in fault zones (Green & Burnley 1990, Burnley *et al.* 1991).

The principal goal of this study was to measure the sliding resistance on faults generated by the anticrack mechanism as a function of confining pressure. The observed pressure and rate dependence of the sliding stress indicate that sliding is not controlled by friction. It appears that sliding occurs by a viscous process induced by the extremely fine grain size of the high density phase that grows in the anticracks and is incorporated into the

*Present address: Department of Geology, Stanford University, Stanford, CA 94305, U.S.A.

†Also at: Lamont-Doherty Geological Observatory of Columbia University, Palisades, NY 10964, U.S.A. Present address: Institute of Geophysics and Planetary Physics, University of California, Riverside, CA 92521, U.S.A.

Table 1. Experimental data for faulted Mg_2GeO_4 specimens

Sample	P (MPa)	T_1 (K)	T_2 (K)	Faulting stress (MPa)	Sliding stress (MPa)	Strain rate (s^{-1})
GB13	1069	1246	1245	877	230	1.4×10^{-4}
GB18	1076	1221	1209	727	384	1.7×10^{-4}
GB28*	1055	1239	1233	1415	251	1.1×10^{-4}
GB29*	1183	1239	1238	1050	185	1.3×10^{-4}
GB31*	2190	1238	1207	1021	499	1.5×10^{-4}
GB36*	1751	1245	1238	1024	543	1.7×10^{-4}
GL299†	1154	1201	1164	933	332	2.1×10^{-4}
GL312†	1135	1199	1183	991	676	2.2×10^{-4}
GL326†	1895	1298	1286	1260	629	2.3×10^{-3}
GL415†	1210	1200	1149	1293	279	2.1×10^{-4}

*Experiments using the second polycrystal described in the text.
†Experimental data reported previously by Burnley *et al.* (1991).

fault zone during faulting. Thus, the underlying physics of the anticrack mechanism of phase-transformation faulting (and, by extension, the mechanism of deep-earthquake faulting) are distinct from those involved in brittle shear failure.

EXPERIMENTAL TECHNIQUES

The starting material for these experiments was synthetic polycrystalline Mg_2GeO_4 olivine with 5 wt% $MgGeO_3$ orthopyroxene. Crystalline olivine and pyroxene germanate powders, synthesized from MgO and GeO_2 powders at 1150°C and 1 atm and subsequent grinding, were isostatically hot-pressed at 200 MPa and 1400°C for 2 h in sealed Fe canisters. The Fe canisters (internal dimensions 6.5 cm diameter and 2 cm thick) were heated, flushed with Ar and then evacuated to minimize incorporation of water and other contaminants into the polycrystal. Two separate polycrystals were used for the new experiments reported here (Table 1); the first polycrystal, described by Burnley *et al.* (1991), was 90–95% dense with a mean grain size of 30 μm. The second polycrystal (Fig. 1) is 98% dense with a mean grain size of 50 μm. In the second synthesis, the germanate powder reacted with the canister producing a thin rind, ~1 mm thick, of Fe and germanate crystals displaying a eutectic-like texture. Diffusion of Fe into the polycrystal was limited to the outer 1–2 mm of the polycrystal; this outer region was not used. The crystal-plastic rheology of the two polycrystals is identical.

Specimens for the new experiments were 3.05–3.18 mm in diameter and 5.6–8.5 mm long. They were rinsed with acetone and dried in vacuum at 120–150°C for several hours and sealed (TIG welded shut) in Pt capsules (0.25 mm thick). The encapsulated specimens were cast into an Inconel 600 sleeve with NaCl; the pressure assembly used for the experiments is depicted in Fig. 3. The pressure assembly differs somewhat from that used in previous experiments reported by Burnley *et al.* (1991), but the slight differences have no effect on the reported mechanical data.

The samples were pressurized at room temperature to 100–200 MPa below the desired pressure and then heated at 5–10 K min^{-1} to 900 K. For some experiments, the sample was then heated at 10–25 K min^{-1} to the desired final temperature; for others, the sample was brought to the final temperature in a matter of a few seconds. Some samples were deformed at a constant piston displacement rate of 1 μm s^{-1} (corresponding to an approximately constant strain rate of 2×10^{-4} s^{-1}), while others were deformed at true constant strain rates of 1×10^{-4}–3×10^{-4} s^{-1}; no discrepancy in the results between the two modes of deformation was noted. The reported stress–strain curves were calculated from the differential stress (axial stress minus the confining pressure) and displacement, assuming a homogeneous, constant-volume, axial shortening (a good approximation up to the point of failure).

It was not possible to perform these experiments in a molten salt, as is the usual practice now in our laboratory, because stresses above 800 MPa (see Fig. 4) generally cause axial splitting of the Al_2O_3 deformation piston (Fig. 3) and rupture of the Pt capsule. Therefore, NaCl was chosen as the confining medium because it would be close to, but below, its melting temperature during the experiments. The level of friction on the deformation pistons was determined by visually fitting straight lines to the differential stress during piston advance and the elastic slope after the piston contacted the specimen. The maximum error introduced by the method is estimated to be about 100 MPa (see Burnley *et al.* 1991 for further discussion). The accuracy of the fit was verified by experiments conducted in molten salt, in which the Pt capsule perforated during the deformation and molten salt intruded the sample. Specimens that fail in this manner have no post-failure strength, and the residual stress after failure was within 100 MPa of the level of friction determined by the method described above.

Acoustic emissions were monitored in some experiments (see Green *et al.* 1992) by placing a miniature piezoelectric transducer (2 mm diameter Valpey Fisher VP1093) against the tungsten carbide (WC) base anvil of the sample assembly (Fig. 3). The transducer was electrically isolated by wrapping it with transparent tape and bonding (silver epoxy) a thin (1–2 mm thick) alumina buffer rod to the end of the transducer in contact with the WC base anvil. The acoustic signals were amplified

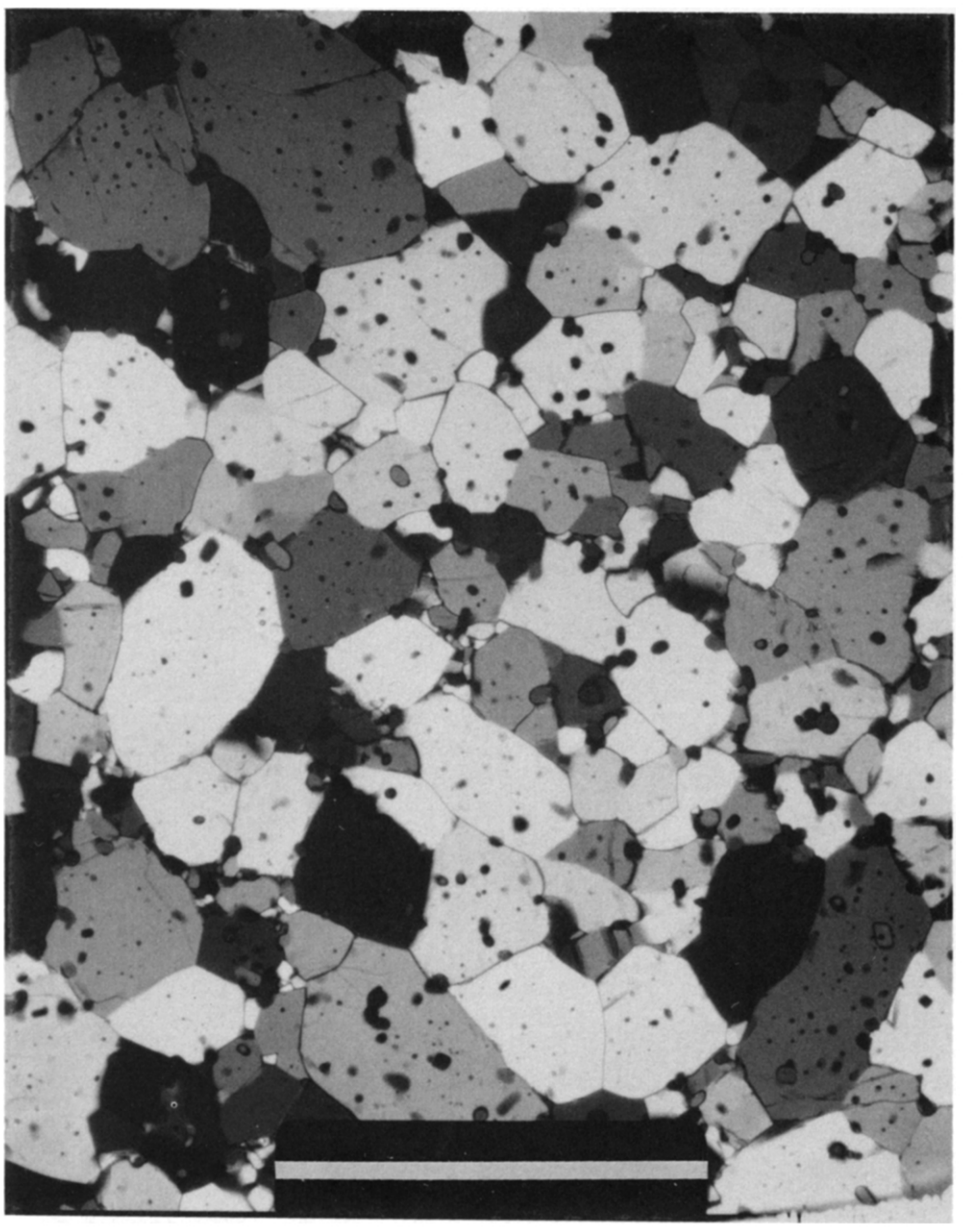

Fig. 1. Photomicrograph (crossed polars) of the second Mg_2GeO_4 olivine polycrystal. The inclusions visible within the larger crystals of this micrograph are $MgGeO_3$ orthopyroxenes. Scale bar = 200 μm.

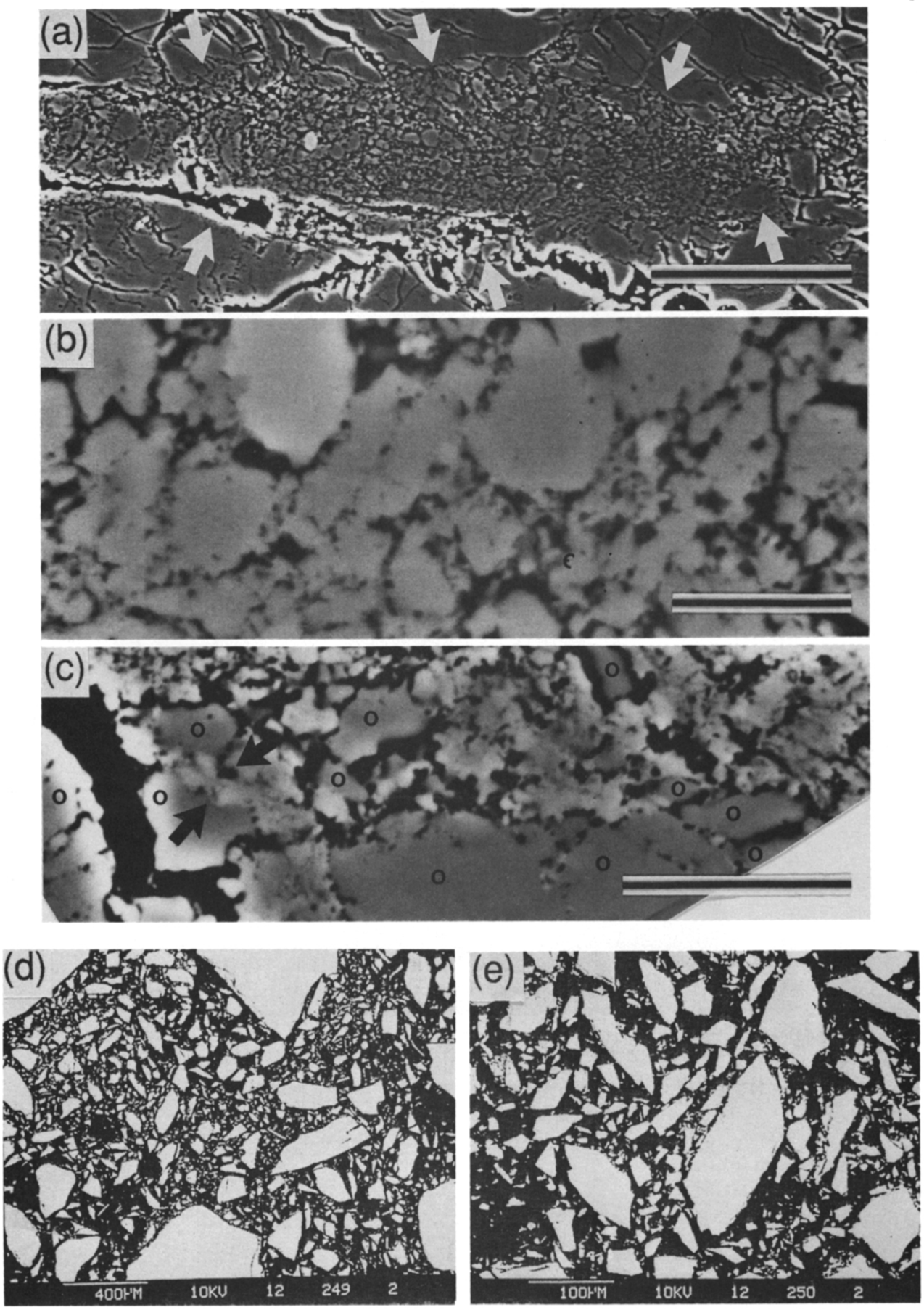

Fig. 2.

75 dB, discriminated and counted. In addition, a Tektronix model 2211 digital oscilloscope was used to record and store waveforms of individual acoustic events.

RESULTS

Experimental data for specimens that were allowed to slide after faulting are reported in Table 1. The amount of strain that preceded faulting is variable; some samples faulted shortly after yielding (e.g. sample GL312, fig. 4 in Burnley *et al.* 1991), while others accumulated natural strains of >40% before failure. In the representative stress–strain curves of Fig. 4, faulting occurred after 30–45% natural strain (axial shortening). The level of stress at the stress drop is referred to hereafter as the faulting stress (Fig. 4a). The level of acoustic activity prior to faulting, also shown in Fig. 4, was indistinguishable from that occurring before the piston made contact with the specimen and is unrelated to deformation (the threshold level of the discriminator was adjusted so that random noise triggered between one and two events s^{-1}). In all cases, the stress drop (measured external to the pressure assembly by a load cell) occurred within a few seconds and was accompanied by a burst of acoustic activity. The samples were allowed to slide after faulting; the level of stress supported by the sample after faulting is referred to hereafter as the sliding stress (Fig. 4a). Acoustic activity after faulting was only slightly higher than the background level established prior to faulting.

Waveforms of two acoustic events recorded during the stress drop in sample GB29 are shown in Fig. 5. The larger of the two events was impulsive and decayed over a period of about 30 μs; the second, smaller event was not as impulsive as the first.

The faulting stress is independent of confining pressure and shows considerable scatter between 700 and 1500 MPa (Table 1, Fig. 6a). The sliding stress also shows significant scatter but appears to be weakly dependent on pressure, varying from about 340 MPa at 1000 MPa confining pressure to about 600 MPa at 2200 MPa confining pressure (Figs. 6a & b).

Sliding stress is strongly dependent on sliding rate. The sliding stress immediately after faulting in specimen GB29 (Fig. 4c) was 185 ± 14 MPa at a piston displacement of 1 μm s^{-1} (corresponding to a sliding rate on the fault of ~1.2 μm s^{-1}). Twice, the piston displacement rate was changed briefly (1 and 5 min duration, respectively) to 0.1 μm s^{-1} (sliding rate ~0.12 μm s^{-1}), and the sliding stress fell to 92 ± 10 MPa within 30 s. In both instances, the sliding stress returned to 180 MPa when the piston displacement rate was increased to 1 μm s^{-1}.

DISCUSSION

Several previously reported observations of the anomalous faulting behavior triggered during the $\alpha \rightarrow \gamma$ phase transformation in Mg_2GeO_4 polycrystals indicated that *initiation* of faulting is not related to brittle shear fracture. (1) The faulting stress is independent of confining pressure, in marked contrast to the pronounced increase with pressure exhibited by brittle failure and predicted by the Mohr–Coulomb fracture criterion (Fig. 6a) (Burnley *et al.* 1991). (2) Faulting occurs only in a narrow temperature interval (Green & Burnley 1989, Burnley *et al.* 1991). At lower temperatures, samples do not transform to spinel (except for the minor production of martensitic lamellae; Burnley & Green 1989) and are ductile and strong. At higher temperatures, samples transform extensively to spinel and are ductile and relatively weak. The mechanical instability correlates with incipient transformation of metastable olivine to spinel. (3) No acoustic emissions occur prior to faulting, and a burst of acoustic activity occurs during the stress drop associated with faulting (Fig. 4) (Green *et al.* 1992). This contrasts markedly to the crescendo of acoustic activity that precedes brittle failure due to the formation of Mode I microcracks (Scholz 1990). In addition, anticrack faulting has been observed at 14 GPa during the $\alpha \rightarrow \beta$ transformation in silicate olivine (Green *et al.* 1990). This also implies that brittle fracture is not involved in this phenomenon because dilatant (i.e. brittle) processes are impossible at such pressures.

On the other hand, direct evidence for the presence or absence of brittle processes *during* or *after* anticrack faulting has been equivocal. Burnley *et al.* (1991) noted that faults which had slipped extensively (more than ~1 mm) exhibited abundant fragments of olivine in the fault zones along with the finer-grained spinel. They speculated that during or after faulting, brittle processes were active and that the pieces of olivine present in fault zones

Fig. 2. Back-scattered-electron images of fault 'gouge' produced by the anticrack mechanism (a–c) compared with images of gouge produced by brittle fracture (d & e) (from Marone & Scholz 1989). (a) Fault zone in GL299 (E–W across micrograph and bounded by white arrows) contains visible fragments of olivine and pyroxene, and fine-grained spinel (not visible at the resolution of this micrograph). Note that pyroxene is brighter in these images owing to its higher electron backscattering coefficient. White-bordered black regions are cracks and plucks produced during sectioning and polishing. Scale bar = 60 μm. (b) Detail of left-center portion of (a) showing bimodal grain-size distribution and rounded, sinuous grain boundaries of olivine (darker gray) and pyroxene fragments, with very fine-grained spinel crystals (lighter gray) between them. Most of the areas between olivine fragments are plucked out because of the contrast in hardness of the phases and the extremely fine grain size of the spinel. Scale bar = 6 μm. (c) Border of one of the fault zones in GL415 showing a much larger fraction of spinel in the fault zone. Note the extremely irregular shapes of the olivine fragments (darker gray; labeled with an 'o'). In particular, note the region near the lower left corner where a zone of spinel (lighter gray and indicated by black arrows) has propagated through an olivine grain. The transformation process appears to be 'carving off' a piece of olivine and leaving it in a matrix of spinel; this may explain why anticrack fault 'gouge' possesses a bimodal grain-size distribution and grains have such irregular margins. Black band at left is a crack produced during sectioning. As in (b), many areas of spinel have been plucked during the polishing process. Scale bar = 10 μm. (d) Gouge from experimental study of frictional sliding in quartz. Note angularity and wide range of sizes. Scale bar = 400 μm. (e) Detail of central-left area of (d), showing self-similarity of particle-size distribution. Scale bar = 100 μm. This fractal distribution contrasts sharply with the bimodal size distribution in (b) and (c).

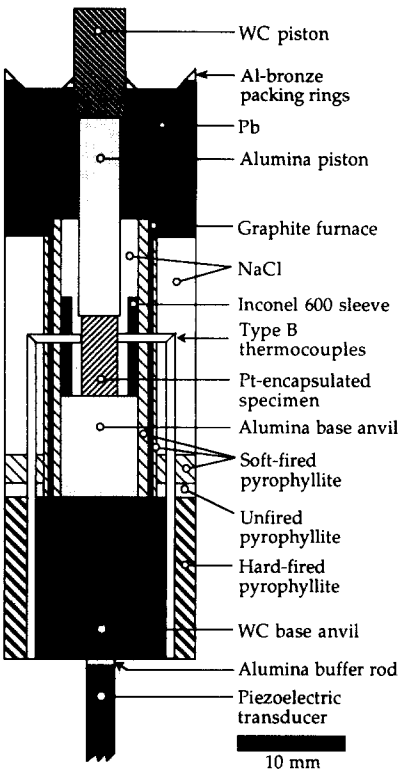

Fig. 3. Schematic drawing of the pressure assembly utilized in the new experiments. The location of the piezoelectric transducer used to monitor acoustic emissions is shown also.

had broken from the borders of the fault and therefore constituted a normal fault gouge. However, Green *et al.* (1992) noted that the fault 'gouge' (see fig. 12 of Burnley *et al.* 1991) differs in certain fundamental respects from experimental (Marone & Scholz 1989) and natural (Sammis *et al.* 1986) fault gouges produced in the brittle regime. Figure 2 shows that comparison directly; anti-crack fault 'gouge' has a bimodal particle-size distribution and the grains have rounded, sinuous margins, whereas brittle fault gouge has a fractal particle-size distribution and grains are highly angular. To explain these characteristics, Green *et al.* (1992) proposed that the olivine fragments in the fault zones were 'carved out' by enhanced local Mode I microanticracking during fault zone propagation and widening (Fig. 2c).

The new data presented here imply that the resistance to sliding on faults generated by the anticrack mechanism is not due to a frictional process. First, the sliding resistance depends only weakly on the normal stress on the fault zone, in contrast to the strong dependence of frictional sliding on normal stress universally observed in brittle materials (Fig. 6b). Second, an order of magnitude increase in the displacement rate caused the sliding stress to roughly double. Even when friction has a positive rate effect (velocity strengthening), as in granular material, the magnitude of that effect is very much smaller than we observed, on the order of 1% change in strength per order of magnitude change in sliding rate (Marone *et al.* 1990). Third, the level of acoustic emissions during sliding is only slightly higher than background; this also is not consistent with a frictional process. Thus, friction is excluded as the process controlling sliding.

To understand the process by which sliding takes place in the spinel-lined fault zones, we compare the results of this study with mechanical data for bulk flow of polycrystalline γ-Mg_2GeO_4. Vaughan & Coe (1981) found that a γ-Mg_2GeO_4 polycrystal with a grain-size of about 2 μm exhibited a stress exponent $n \sim 2$ and concluded that flow probably was dominated by grain-boundary sliding. In contrast, Tingle *et al.* (1991) found that coarser-grained (20–30 μm) γ-Mg_2GeO_4 polycrystals flow by dislocation creep, exhibit a stress exponent $n \sim 3$, and under all conditions are *stronger* than olivine (e.g. at 1200 K, 1800 MPa and strain-rates of 10^{-4} and 10^{-5} s^{-1}, they measured steady-state flow stresses of 1750 and 800 MPa, respectively). Thus, although the rheology of the fault zones has not been fully characterized, it is not compatible with friction *or* with the crystal-plastic rheology of either olivine or spinel. The most

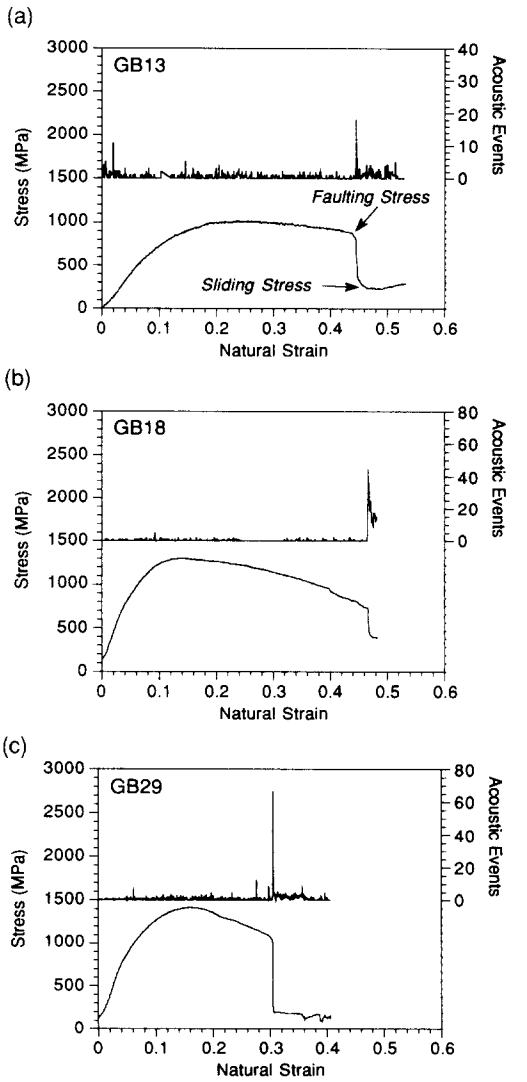

Fig. 4. Stress vs natural strain for experiments (a) GB13, (b) GB18 and (c) GB29 and the accompanying record of acoustic emissions (number of acoustic events s^{-1}). For experiment GB13 only, the acoustic emissions were recorded by a transducer attached to the load frame as discussed by Green *et al.* (1992) which resulted in a lower sensitivity—note the scale difference for the acoustic events recorded between (a) and (b) or (c).

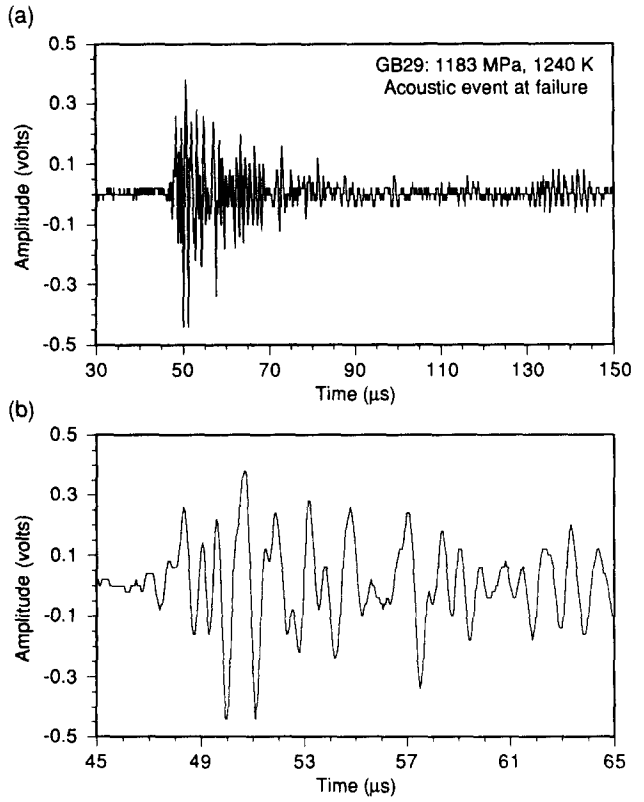

Fig. 5. (a) Digitally recorded waveforms for two acoustic events recorded during the stress drop in experiment GB29. (b) An expanded timebase of the early part of the first event in (a).

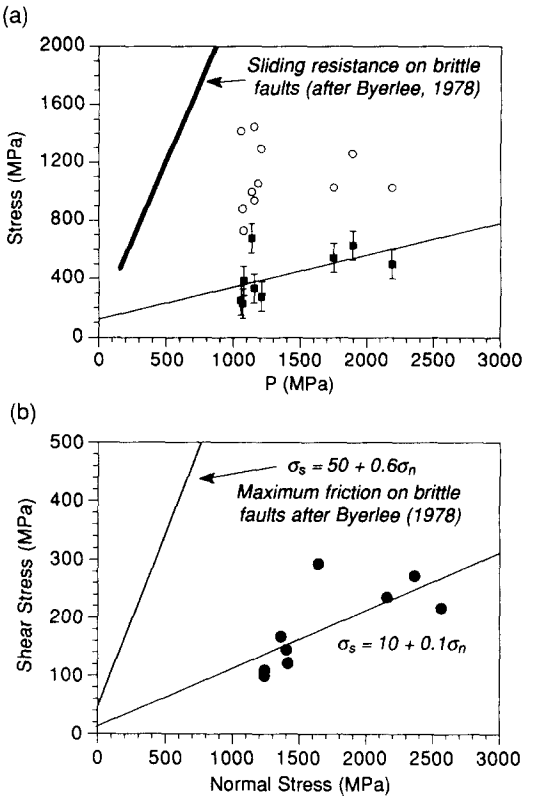

Fig. 6. (a) Faulting stress (open circles) and sliding stress (solid squares) as a function of confining pressure for Mg_2GeO_4 specimens that failed by the anticrack mechanism. Experimental data are in Table 1. As discussed in the text, the sliding stress data were estimated to have a maximum uncertainty of ± 100 MPa (error bars). The bold line shows the expected increase in sliding resistance with confining pressure for brittle faults oriented at 30° to the maximum compressive stress (after fig. 1-12, Scholz 1990, data from Byerlee 1978). (b) Shear stress vs normal stress calculated from the sliding stress data in (a) and in Table 1 assuming faults oriented at 30°. In detail, the faults were not planar and varied from 25° to 35°. Linear regression of the experimental data yields σ_s (MPa) = 10 + 0.1σ_n. Byerlee's law (Byerlee 1978) for frictional sliding on brittle faults in a wide variety of materials is shown also for comparison.

reasonable interpretation is that sliding occurs by grain-boundary sliding of the very fine-grained spinel that separates the olivine fragments in the 'gouge' (Figs. 2b & c). The pressure- and rate-dependence of the sliding stress are compatible with such a viscous process.

CONCLUSIONS

This investigation confirms that initiation of faulting by the anticrack mechanism in Mg_2GeO_4 is not related to brittle failure (Burnley *et al.* 1991) and further shows that sliding after faulting is not controlled by brittle processes. The pressure- and rate-dependence of the sliding stress and the microstructures of the fault zones are consistent with the hypothesis that the rheology of faults triggered by the olivine → spinel phase transformation is controlled by grain-boundary sliding in the fine-grained spinel of the fault zones. Given that initiation and sliding of such faults are not brittle phenomena, it seems unlikely that fault *propagation* is a brittle process either. Thus, the physical processes responsible for anticrack faulting in Mg_2GeO_4 are fundamentally different from those responsible for brittle shear fracture.

These results add to a growing body of evidence that incipient transformation of metastable silicate olivine to β-phase (or spinel) in lens-shaped microanticracks that organize themselves into throughgoing faults is the mechanism of deep-earthquake faulting. Iidaka & Suetsugu (1992) provided evidence that olivine exists metastably to a depth of at least 500 km in the cold interior of the Pacific lithospheric slab being subducted beneath Japan, and Green *et al.* (1990) showed that anticrack faulting can accompany the $\alpha \rightarrow \beta$ transformation in $(Mg,Fe)_2SiO_4$ at the high pressures at which deep-focus earthquakes occur. Microstructures of the faulted silicate specimen are essentially identical to those of the germanate specimens, and we expect that the rheology and acoustic emissions (seismic) characteristics of faults triggered by the anticrack mechanism during the $\alpha \rightarrow \beta$ transformation in $(Mg,Fe)_2SiO_4$ will be similar. The reader should not conclude, however, that deep faults will slip extensively by superplastic processes after an earthquake. The fine-grained β-phase or spinel in fault zones probably will coarsen rapidly on a geological time scale and thus leave the nascent fault zones stronger than their untransformed country rock.

Acknowledgements—We thank P. C. Burnley for providing the unpublished stress–strain data from her experiment GL299, J. A. Abril for preparation of the experimental assemblies and for constant maintenance and repair of the apparatus, and T. E. Young for helpful discussions and assistance with the apparatus and some of the experiments. A. G. Sylvester and N. L. Carter provided thorough and constructive reviews. H. W. Green extends a special thanks to John Christie who, as mentor and friend during his years in graduate school,

provided education, encouragement and inspiration that have been of lasting assistance over the succeeding 25 years. This work was supported by NSF grants EAR89-05059 and EAR89-15938. LDGO contribution No. 5008.

REFERENCES

Burnley P. C. & Green, H. W. 1989. Stress dependence of the mechanism of the olivine–spinel transformation. *Nature* **338**, 753–756.

Burnley, P. C., Green, H. W., II & Prior, D. J. 1991. Faulting associated with the olivine to spinel transformation in Mg_2GeO_4 and its implications for deep-focus earthquakes. *J. geophys. Res.* **96**, 425–443.

Byerlee, J. 1978. Friction of rocks. *Pure & Appl. Geophys.* **116**, 615–626.

Green, H. W. & Burnley, P. C. 1989. A new, self-organizing, mechanism for deep-focus earthquakes. *Nature* **341**, 733–737.

Green, H. W. & Burnley, P. C. 1990. The failure mechanism for deep-focus earthquakes. In: *Deformation Mechanisms, Rheology and Tectonics* (edited by Knipe, R. J. & Rutter, E. H.). *Spec. Publs geol. Soc. Lond.* **54**, 133–141.

Green, H. W., II., Scholz, C. H., Tingle, T. N., Young, T. E. & Koczynski, T. A. 1992. Acoustic emissions produced by anticrack faulting during the olivine → spinel transformation. *Geophys. Res. Lett.* **19**, 789–792.

Green, H. W., II, Young, T. E., Walker, D & Scholz, C. H. 1990. Anticrack-associated faulting at very high pressure in natural olivine. *Nature* **348**, 720–722.

Iidaka, T. & Suetsugu, D. 1992. Seismological evidence for metastable olivine inside a subducting slab. *Nature* **356**, 592–595.

Kirby, S. H. 1987. Localized polymorphic phase transformation in high-pressure faults and applications to the physical mechanism of deep focus earthquakes. *J. geophys. Res.* **92**, 13,789–13,800.

Kirby, S. H., Durham, W. B. & Stern, L. 1991. Mantle phase changes and deep-earthquake faulting in subducting lithosphere. *Science* **252**, 216–225.

Marone, C. & Scholz, C. H. 1989. Particle-size distribution and microstructures within simulated fault gouge. *J. Struct. Geol.* **11**, 799–814.

Marone, C., Raleigh, C. B. & Scholz, C. H. 1990. Frictional behavior and constitutive modeling of simulated fault gouge. *J. geophys. Res.* **95**, 7007–7025.

Sammis, C. G., Osborne, R., Anderson, J., Banerdt, M. & White, P. 1986. Self-similar cataclasis in the formation of fault gouge. *Phys. Earth & Planet. Interiors* **124**, 53–78.

Scholz, C. H. 1990. *The Mechanics of Earthquakes and Faulting.* Cambridge University Press, New York.

Tingle, T. N., Green, H. W. & Borch, R. S. 1991. High-temperature creep experiments on the olivine and spinel polymorphs of Mg_2GeO_4: Implications for the rheology of the Earth's mantle. *Eos* **72**, 297.

Vaughan, P. & Coe, R. S. 1981. Creep mechanism in Mg_2GeO_4: Effects of a phase transition. *J. geophys. Res.* **86**, 389–404.